Journal of Materials Chemistry A

Designer hydrogenated wrinkled Yolk@Shell TiO2 architectures: towards advanced room temperature visible light selective photocatalysts

Journal:	*Journal of Materials Chemistry A*
Manuscript ID	Draft
Article Type:	Paper
Date Submitted by the Author:	n/a
Complete List of Authors:	Ziarati, Abolfazl; School of Chemistry, College of Science, University of Tehran, chemistry Badiei, Alireza; School of Chemistry, College of Science, University of Tehran, chemistry Luque, Rafael; Universidad de Cordoba, Departamento de Quimica Organica Ouyang, Weiyi; Universidad de Cordoba, Departamento de Quimica Organica

Dear Prof. Qiao

Pleased to contact you, I hope this message finds you well. We are delighted to submit the manuscript entitled "Designer hydrogenated wrinkled Yolk@Shell TiO2 nanoarchitectures: towards advanced room temperature visible light selective photocatalysts" to be considered for publication in Journal of Materials Chemistry A.

The manuscript discloses the preparation of an unprecedented yolk/shell wrinkled TiO2 architectures with excelling photocatalytic activities under visible light irradiation. This method includes solvothermal, partial etching and hydrogen treatment sequential preparation steps. The resultant yolk@hydrogenated wrinkled shell TiO2 architectures exhibited a high efficiency in visible light oxidation of alcohols to the corresponding aldehydes (up to 90 in conversion, 97% in selectivity).

We believe this work can be of importance and interest to the broad readership of the journal and look forward to hearing from you soon in this matter.

With best wishes

Prof. Rafa Luque

Journal of Materials Chemistry A

ARTICLE

Designer hydrogenated wrinkled Yolk@Shell TiO_2 architectures: towards advanced room temperature visible light selective photocatalysts

Received 00th January 20xx,
Accepted 00th January 20xx

DOI: 10.1039/x0xx00000x

www.rsc.org/

Abolfazl Ziarati, [a] Alireza Badiei,*[a] Rafael Luque,*[b, c] Weiyi Ouyang, [b]

Smart architectures of TiO_2 are attracting increasing attention due to their outstanding properties in a broad range of fields. Herein, we report the preparation of an unprecedented yolk/shell wrinkled TiO_2 architecture with excelling photocatalytic activities under visible light irradiation. This method includes solvothermal, partial etching and hydrogen treatment sequential preparation steps. The solvothermal step lead to yolk@shell TiO_2 (Y@S-TiO_2) structures which can generate a multi reflection of incident light so as to promote an efficient light harvesting due to an enhanced surface area and light scattering ability based on the hydrothermal alkaline partial etching. The hydrogen treatment process generated Ti^{3+} species on the surface of TiO_2 which facilitate electron-hole separation, decreasing the band gap of titania to visible region. The resultant yolk@hydrogenated wrinkled shell TiO_2 architecture exhibited a high efficiency in visible light oxidation of alcohols to the corresponding aldehydes (up to 90 in conversion, 97% in selectivity).

Introduction

TiO_2 has received broad attention as a favourable candidate for use in water splitting, dye-sensitized solar cells and photocatalysis reactions in recent years due to its outstanding chemical and physical properties including photo-corrosion resistance, chemical stability, low toxicity and suitable electronic band structure.[1-4] The ability to adjust nanostructured TiO_2 to diverse polymorphs and morphologies is the key to efficiently design advanced functional materials for the aforementioned applications.[5-7]

Several TiO_2 morphologies have been extensively investigated including nanotubes, nanowires, hollow spheres, core/shell and yolk@shell architectures.[8-14] Yolk@shell architectures have attracted particular attention and emerged as a modern generation of smart functional structures.[15, 16] These structures generally include a functional core and a hollow porous shell. Owning to their unique structural properties including the presence of interstitial hollow spaces, the permeability of shells and the tunable functionalities in both the inner core and outer shell, yolk@shell architectures have been employed in various fields such as biomedicine, sorption, electrochemistry, catalysis and especially in energy conversion.[17-22] For example, Li *et al.* have prepared TiO_2 mesoporous yolk@shell microspheres with high light scattering ability.[23] Feng *et al.* synthesized Y@S-TiO_2 structures composed of single anatase TiO_2 phase with high light conversion abilities.[24]

All reported yolk@shell structures displayed an improved light harvesting activity as compared to commercial TiO_2 because of their larger high specific surface areas and light-scattering abilities.

A large diversity of living organisations with wrinkled structures can be found in nature. These include plant seeds, pollens and several microorganisms. Wrinkled structures can provide large surface areas which improve surface properties including tracking, adhesiveness and capturing functions. Furthermore, the structural stability and light utilization efficiency has been reported to be improved in wrinkled surfaces.[25] Inspired by such concept in nature, this contribution was aimed to design artificial wrinkled surfaces based on Y@S-TiO_2 structures as advanced functional photonanocatalysts.

The development of stable and highly active visible light absorption titania photocatalysts still remains a significant challenge since TiO_2 uses are critically hindered by ineffective operation of visible light (43% of total solar energy) which results from its wide band gap (3.2 eV). The preparation of reduced TiO_2 nanomaterials containing Ti^{3+} species has been considered as a promising environmentally friendly strategy to enhance visible light photoactivity.[26-31] In fact, hydrogenated

[a] School of Chemistry, College of Science, University of Tehran, Tehran, Iran
[b] Departamento de Quimica Organica, Universidad de Cordoba, Campus de Rabanales, Edificio Marie Curie, E-14014 Cordoba, Spain, e-mail:
E-mail: abadiei@khayam.ut.ac.ir, rafael.luque@uco.es
[c] Peoples Friendship University of Russia (RUDN University) 6 Miklukho-Maklaya str., Moscow, 117198, Russia
Fax: +98-21-61112614; Tel.: +98-21-61112614
Electronic Supplementary Information (ESI) available: [details of the Materials and apparatus used, formation process of Y@S-TiO_2 microspheres, UV-Vis spectra and nitrogen adsorption-desorption isotherms of some of structures, and the reusability study of Y@HWS-TiO_2 architecture]. See DOI: 10.1039/x0xx00000x

TiO_2 nanostructures exhibiting even a disordered surface have already been reported to have an improved light absorption.[32] The improved photocatalytic efficiencies of hydrogenated TiO_2 have been ascribed to the role of surface Ti–H bonds in modifying optical absorption and a more effective photo generated electron–hole separation.[33, 34] In other cases, greater photo activities of reduced TiO_2 nanocrystals have been related to the presence of oxygen vacancies.[35] Moderate to high concentrations of Ti^{3+} on the surface of reduced TiO_2 have been proposed to be important in creating a facile transfer of an electron or hole.[36]

Based on these premises, and following research endeavours from our groups,[37-42] herein we report an unprecedented strategy for the rational design of advanced yolk@hydrogenated wrinkled shell titania (Y@HWS-TiO_2) nanoarchitectures as selective and efficient visible light photonanocatalysts for the selective oxidation of alcohols at room temperature.

Experimental

Synthesis of yolk@shell TiO_2 structures: The Y@S-TiO_2 structures were prepared according to the literature.[24]

Synthesis of yolk@ wrinkled shell TiO_2: The Y@WS-TiO_2 microspheres were synthesized through an alkaline hydrothermal partial etching process. The above obtained Y@S-TiO_2 microsphere (0.5 g) were mixed with an aqueous NaOH solution (12 mL, 1.0 M) and vigorously stirred for 20 min and sonicated for 10 min. Then the suspension was added into a Teflon-lined stainless-steel autoclave (18 mL in capacity). The autoclave was heated at 150 °C for different times, and then allowed to cool to room temperature naturally and the product was isolated by centrifugation. After that, the precipitate was immersed in a dilute HCl (100 mL, 0.1 M) for 5 min and then washed with deionized water until pH value was close to 7, and then dried at 80 ºC for 12 h.

Synthesis of yolk@ hydrogenated wrinkled shell TiO_2: The resulting Y@WS-TiO_2 microspheres were calcined at 550 ºC (the heating rate is 3 ºC/min) for 3 h at 200 psi flow rate under H_2/Ar (1:1) atmosphere. At the end of the heating period, the sample was cooled to room temperature naturally under H_2/Ar atmosphere, named Y@HWS-TiO_2.

Photocatalytic experiments: Visible light photocatalytic reactions were done in a parallel photoreaction cells (12 × 5 mL) made of Pyrex glass with the continuous O_2 bubbling (10 psi flow rate) and water circulation to control the temperature (25 ºC) during the experiments. A halogen lamp (Osram, 220 V and 500 W) was used as the visible light source.

UV light photocatalytic reactions were carried out at room temperature in a batch quartz reactor with the continuous O_2 bubbling (10 psi). Artificial irradiation was provided by a 15 W (UV–C) mercury lamp (Philips, Holland) emitting around 254 nm, positioned in top of the batch quartz reactor.

For each experiment, 5 mg of catalyst was dispersed in the mixed solution of benzyl alcohols (0.3 mmol) and acetonitrile (3 mL) under continuous O_2 bubbling. Prior to light irradiation, the mixtures were stirred for 1 h in the dark to gain the adsorption–desorption equilibrium for benzyl alcohols and dissolved oxygen on the surface of photocatalyst. The photocatalytic reactions were carried out in 12 parallel reaction cells (To have the same conditions in all reactions) under magnetic stirring in presence of light for 3h. At the end of reaction, about 1 mL of suspension was withdrawn and centrifuged to remove the remained catalysts. The concentrations of benzyl alcohols and benzaldehydes were measured with GC-FID or HPLC.

Results and discussion

Preparation and characterization of Y@HWS-TiO_2 architectures

The synthesis procedure of the Y@HWS-TiO_2 architectures includes the following main steps: 1) solvothermal preparation of Y@S-TiO_2, 2) alkaline hydrothermal partial etching to produce Y@S-TiO_2 with wrinkled shell (Y@WS-TiO_2), and 3) hydrogen treatment procedure to achieve Y@HWS-TiO_2 architectures. Fig. 1 shows a schematic depiction of the process and the corresponding SEM images of synthesized structures from each step.

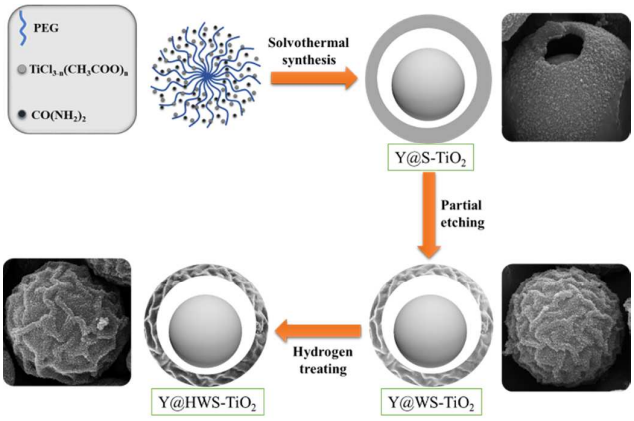

Fig. 1. Overall flowchart for fabrication of the Y@HWS-TiO_2 *via* three sequential steps

Y@S-TiO_2 structure was prepared *via* a one-pot solvothermal method in the presence of polyethylene glycol as a soft template (Fig. S1, Supporting Information). The obtained Y@S-TiO_2 structure exhibited uniformly spherical shape and a mean diameter of ca. 2.8 µm.

Unique wrinkled yolk@shell microspheres were subsequently obtained after hydrothermal etching process in NaOH solution. To provide additional insights into the formation of Y@WS-TiO_2, time-dependent experiments were carried out (Fig. 2). As shown in Fig. 2a, the initial Y@S-TiO_2 structure has a smooth surface. After alkali-hydrothermal process (150 ºC, 1 h), a rough surface could be observed (Fig. 2b). With continuous

hydrothermal etching process for 2 h, a well-developed Y@WS-TiO_2 nanostructure was formed (Fig. 2c) with further thinning and perforation after prolonged etching time (ca. 3 h, Fig. 2d).

A stable Y@HWS-TiO_2 architecture was obtained upon calcination at 500 ºC for 3 h under H_2/Ar atmosphere of optimum Y@WS-TiO_2 (3h alkaline treatment). Fig. 3 depicts the unique wrinkled nanoarchitecture of Y@HWS-TiO_2. A number of Y@HWS-TiO_2 microspheres are evenly distributed as illustrated in FESEM images (Fig. 3a).

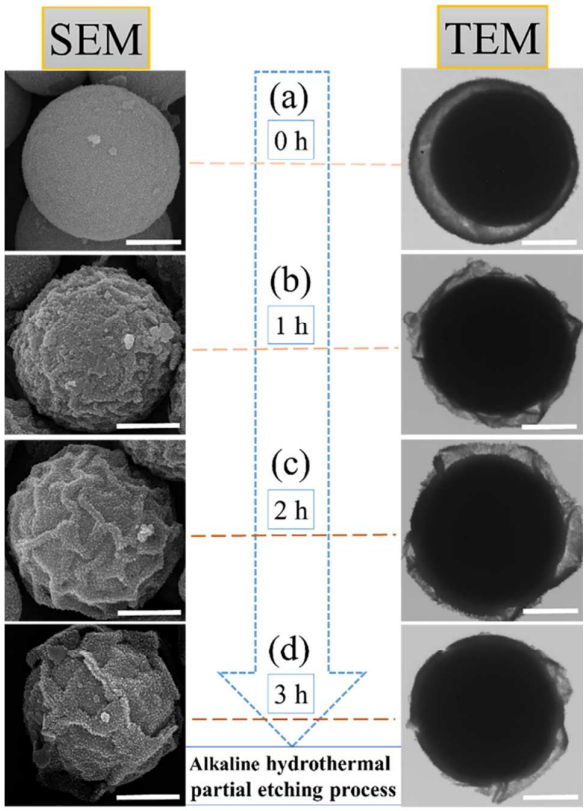

Fig. 2. Alkaline hydrothermal partial etching process of Y@WS-TiO_2 structure at different times. The scale bars are 1 µm.

High magnification micrographs (Fig. 3b) further confirmed the clearly visible presence of wrinkled surfaces randomly assembled on the surfaces of microspheres. From cracked Y@HWS-TiO_2 (Fig. 3c), the outer spherical shell can be visualized to comprise of ultrathin structures. Compared to the outer shell, the inner core has a smoother surface owing to less diffusion of the alkaline etching agent in the inner layer. SEM-BSE micrographs (Fig. 3d) showed a transparent wrinkled shell encapsulating a solid core that further confirm the formation of Y@HWS-TiO_2 nanostructures.

In order to investigate the elemental distribution in Y@HWS-TiO_2 nanoarchitectures, the elemental mappings of Ti and O were carried out by EDS area scanning as shown in Fig. 3e,f. Detailed Y@S-TiO_2 and Y@HWS-TiO_2 microstructures were also further investigated by TEM and HRTEM (Fig. 4). A clear yolk@shell structure could be observed for Y@S-TiO_2 (Fig. 4a) the with void spaces between the inner core and the outer shell. Fig. 4b also supports the wrinkled shell arrangement in Y@HWS-TiO_2. HRTEM images of Y@S-TiO_2 (Fig. 4c) and

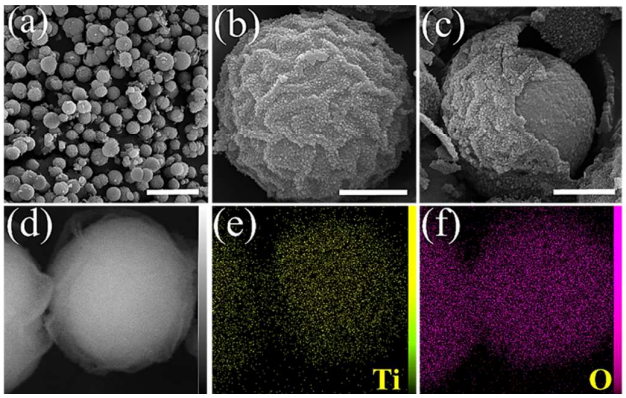

Y@HWS-TiO_2 nanoarchitectures (Fig. 4d) show that both structures have good crystallization with a lattice spacing of 0.35 nm between

Fig. 3. a-c) FESEM d) BSE-SEM, and e,f) EDS mapping images of the Y@HWS-TiO_2. The scale bars are 10 µm (a) and 1 µm (b,c).

(101) TiO_2 planes (red arrows). Furthermore, a thin disordered surface layer encircling the crystalline structure could also be clearly observed (white arrows, Fig. 4d). This can be attributed to the effect of hydrogen treatment and the generation of Ti^{3+} species near the surface as later on confirmed by XPS.[43, 44]

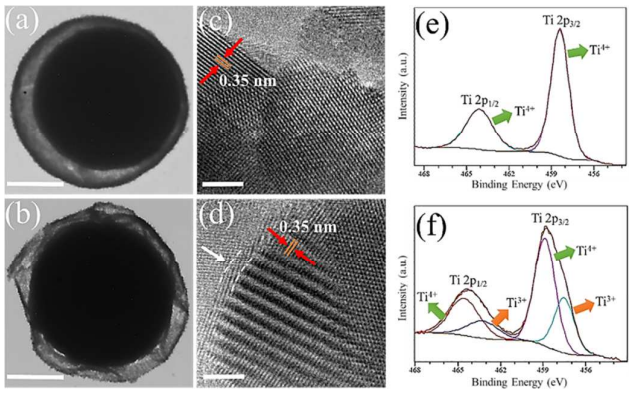

Fig. 4. TEM images of a) Y@S-TiO_2 and b) Y@HWS-TiO_2. HRTEM images of c) Y@S-TiO_2 and d) Y@HWS-TiO_2. XPS Ti 2p spectra of e) Y@S-TiO_2 and f) Y@HWS-TiO_2. The scale bar 1 µm (a,b) and 5 nm (c,d).

The oxidation state and metal components in Y@HWS-TiO_2 were further studied by XPS analysis as compared to on the surface of the material, because the escape depth of electrons is a few nanometres. Two peaks corresponding to Ti $2p_{3/2}$ and Ti $2p_{1/2}$ (ca. 458-465 eV) can be observed in the high resolution Ti 2p XPS spectra of Y@S-TiO_2 and Y@HWS-TiO_2. After deconvolution, Ti 2p peaks of Y@HWS-TiO_2 are divided into four peaks at 457.6 eV, 458.8 eV, 463.3 eV and 464.6 eV. The peaks at 458.8 and 464.6 eV can be assigned to $2p_{3/2}$ and $2p_{1/2}$

core levels of Ti^{4+},[45] whereas the peaks at 457.6 and 463.3 eV are attributable to $2p_{3/2}$ and $2p_{1/2}$ core levels of Ti^{3+},[46] respectively. This clearly reveals the existence of Ti^{3+} ions on the surface of Y@HWS-TiO_2. The relative content of Ti^{3+} ions is roughly calculated to be 32% by comparing the XPS peak areas of Ti^{3+} vs Ti^{4+}.

Raman spectra were measured to investigate potential structural changes on the surface of Y@S-TiO_2 before and after hydrogen treatment (Fig. 5a). Raman spectra indicate notable differences, and two features should be considered. Firstly, the diffraction peaks become weaker after hydrogen treatment. Secondly, the two Eg modes of Y@S-TiO_2 are shifted to higher frequencies in Y@HWS-TiO_2. These two features further confirmed the increase of Ti^{3+} ions in the lattice structure of Y@S-TiO_2 architecture after hydrogenation.[47]

Fig. 5b depicts XRD patterns of Y@S-TiO_2 and Y@HWS-TiO_2 nanoarchitectures. The anatase phase of Y@S-TiO_2 is confirmed to be preserved upon hydrogenation treatment. The sharp anatase (101) reflection of Y@HWS-TiO_2 compared with that of Y@S-TiO_2 can be attributed to the growth of crystallinity during the high temperature hydrogenation process. The diffraction lines of Y@HWS-TiO_2 could be observed to be slightly shifted towards higher diffraction angles, suggesting the reduction of the interplanar distance of the crystalline phase. This result demonstrates that structural changes have occurred in TiO_2 during the hydrogenation process.[48, 49]

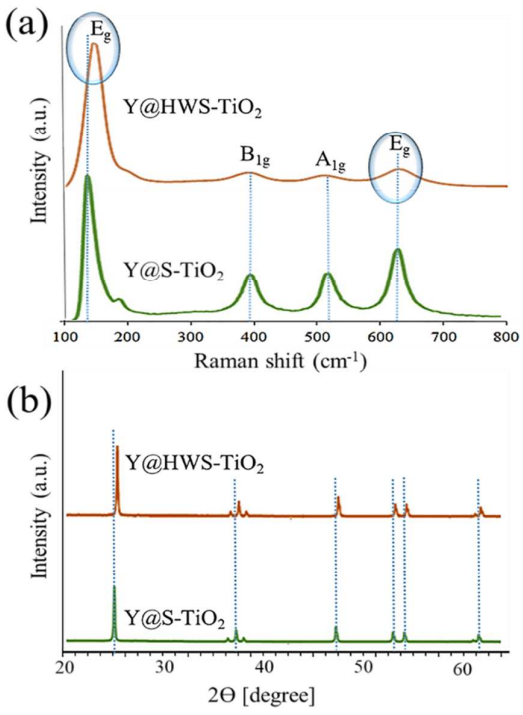

Fig. 5. a) Raman spectra of Y@S-TiO_2 and Y@HWS-TiO_2 and b) XRD patterns of Y@S-TiO_2 and Y@HWS-TiO_2.

UV-vis absorption spectra were measured to confirm the photoactive properties of Y@HWS-TiO_2 as presented in Fig. S2a (Supporting Information). No considerable response could be observed in the C-TiO_2 spectrum in the visible light range (400 and 700 nm). Comparably, the spectrum of Y@HWS-TiO_2 exhibited a strong absorption response in the visible region, possibly related to the presence of Ti^{3+} species on the wrinkled surface.

A new energy level may be created due to the presence of Ti^{3+} ions below the conduction band, resulting in the observed response in the visible region. These results indicate that visible light can in principle activate Y@WS-TiO_2 nanoarchitectures, and more electrons and holes may be produced in photocatalytic reactions. The calculated energy of the band gap of Y@HWS-TiO_2 from the UV-vis spectrum is 2.62 eV (Fig. S2b, Supporting Information)).

To obtain an insight into the porosity of Y@HWS-TiO_2, BET surface areas and pore-size distributions using nitrogen adsorption and desorption isotherms were conducted. Y@S-TiO_2 and C-TiO_2 were tested here as benchmark. Y@HWS-TiO_2 possessed a high BET surface area (276 $m^2.g^{-1}$), nearly five times that of C-TiO_2 (41 $m^2.g^{-1}$) and ca. 60% higher than Y@S-TiO_2 (181 $m^2.g^{-1}$), see Fig. S3, Supporting Information. The isotherms corresponding to Y@HWS-TiO_2 exhibit the typical type IV shape according to the IUPAC classification, revealing a hysteresis loop at high relatively pressures associated with capillary condensation within mesopores. This result demonstrates that porosity overall changes for Y@HWS-TiO_2, with mesopore development and enhanced surface areas.

Photocatalytic activity

The unique hydrogenated wrinkled yolk@shell architecture with high surface area, hollow space between inner core and outer shell (which could act as a porous nanoreactor) as well as visible light activity make Y@HWS-TiO_2 highly suitable for photocatalytic applications. The photocatalytic performance of Y@HWS-TiO_2 was tested in the selective oxidation of benzyl alcohol. Fig. 6 shows that all synthesized TiO_2 samples possess some oxidation photoactivity in the selected test reaction under UV irradiation Interestingly, C-TiO_2, Y@S-TiO_2 and Y@WS-TiO_2 displayed a low photocatalytic activity in the benzyl alcohol photo-oxidation under visible light. Y@HWS-TiO_2 prepared by partial etching and hydrogen treating of Y@S-TiO_2 comparably exhibited a remarkable photocatalytic activity (88% conversion), over a 17-fold increase to that observed for C-TiO_2. More interestingly, no considerable over-oxidation products (e.g. benzoic acid, observed for C-TiO_2) were detected for Y@HWS-TiO_2 under the investigated

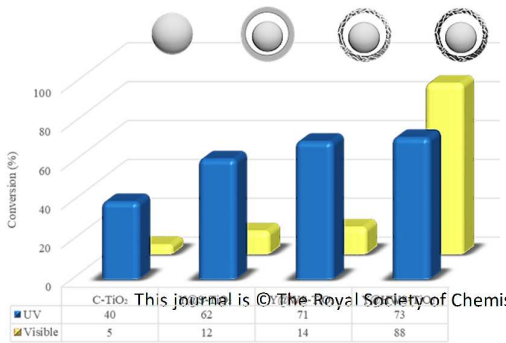

reaction conditions.

Fig. 6. Comparison photocatalytic activity of C-TiO_2, Y@S-TiO_2, Y@WS-TiO_2 and Y@HWS-TiO_2 structures in selective oxidation of benzyl alcohol at UV and visible conditions.

The observed unprecedented photocatalytic activity of Y@HWS-TiO_2 under visible light irradiation may be attributed to five important features present in the system under visible light : 1) a high porosity and hollow space in yolk@shell structure, beneficial for the transportation and adsorption of organic molecules (e.g. benzyl alcohols); 2) the thin wrinkled shell, which may facilitate molecular diffusion and create active sites exposed to reactants; 3) the presence of Ti^{3+} species on the surface of Y@WS-TiO_2 which reduce the band gap of TiO_2 to visible region; 4) the difference in band gaps in TiO_2 core and hydrogen-treated wrinkled shell which promotes electron-hole separation; and 5) the reflecting and scattering of light inside Y@HWS-TiO_2 and on the wrinkled surface which enhances light adsorption by the substrates.
Fig. 7a illustrates the possible reflecting and scattering of light in Y@HWS-TiO_2 nanoarchitectures. It is believed that the light inside the wrinkled shell can be reflected by the inner core several times, with additional scattering the incident light of different wavelengths in the whole range of visible light by the assembled outer shell, these being very appropriate for the adsorption of more light by the photocatalyst as well as the organic substrates (blue and red spots).[24]

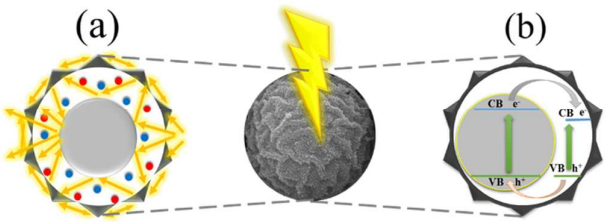

Fig. 7. a) Schematic diagram of the light scattering effect caused by Y@HWS-TiO_2 and b) schematic of the valence and conduction band alignment mechanism for Y@HWS-TiO_2 architecture

To investigate the effect of the introduction of Ti^{3+} species, a schematic of a proposed photocatalytic mechanism of Y@HWS-TiO_2 nanoarchitectured under visible light is provided. The introduced Ti^{3+} species can generate sublevel states, which decrease the band gap of TiO_2. As shown in Fig. 7b, the electron is excited to the impurity level in hydrogenated wrinkle shell upon illumination with visible light. The life of the photo induced electron in the oxygen vacancy trap is much longer as compared to that on the conductive band, which can desirably reduce oxygen and produce a superoxide radical, improving photocatalytic alcohol oxidation efficiency. The holes left in the valence band accelerate the generation of free OH radicals, likely responsible for the enhanced photocatalytic alcohol oxidation activity.[50, 51]
The scope of the oxidation reaction was finally studied using aromatic alcohols and results are summarized in Table 1.

Table 1. Photocatalytic selective oxidation of alcohols promoted by Y@HWS-TiO_2

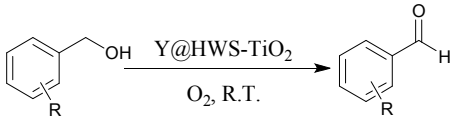

R	T[h]	Light	Conversion (%)	Selectivity (%)
H	3	visible	88	97
		UV	73	96
4-Me	3	visible	86	95
		UV	67	94
4-OMe	3	visible	88	95
		UV	66	91
4-NO_2	3	visible	87	93
		UV	64	92
4-Cl	3	visible	90	97
		UV	71	95
3-Me	3	visible	84	93
		UV	62	91

Since the stability of the catalyst is a crucial item in the photocatalytic reactions, the recovery and reusability of Y@HWS-TiO_2 architecture was also investigated in benzyl alcohol oxidation. Interestingly, this architecture exhibited excellent photocatalytic activity even after five consecutive runs (Fig. S4, Supporting Information), with no detectable leaching of active species (Ti) or structure modification. This outstanding durability can be attributed to its robust wrinkled architectures against chemical and structural collapse, as verified by XRD and FESEM since all chemical and morphological structures of Y@HWS-TiO_2 were almost fully preserved after the 5^{th} recycle.

Conclusions

A new solvothermal, partial etching and hydrogen treatment sequential process for the synthesis of Y@HWS-TiO_2 architecture with large surface area of ~276 m^2g^{-1} and high photocatalytic activity was demonstrated. This method involves the solvothermal step to generate TiO_2 with yolk@shell structures, followed by alkali-hydrothermal partial etching to create wrinkled assemblies on the yolk@shell structure, and finally high temperature hydrogen treatment to generate Ti^{3+} species on the surface of yolk/wrinkle shell TiO_2. Wrinkled hydrogenated yolk@shell architecture of spheres remarkably improved the photocatalytic activity in selective

photooxidations and compared to typical photocatalysts. The presence of Ti^{3+} on the surface reduced the band gap and provided light absorption in the visible region, facilitating electron-hole separation. The proposed strategy led to excellent activity and selectivity in oxidation of alcohols towards the corresponding aldehydes during the whole visible light photocatalytic reaction process. This work can pave the way to additional advances in the design of advanced nanoarchitectures with greatly improved photoactivities (e.g. hydrogen production, solar cells, and solar enhanced fuel cells) that will be reported in due course.

Conflicts of interest

There are no conflicts to declare.

Acknowledgements

The authors thank University of Tehran and funding from the European Union's Horizon 2020 research and innovation programme under the Marie Sklodowska-Curie grant agreement No 641861 (for funding Weiyi Ouyang Ph.D. studies). The publication has been prepared with support of RUDN University Program 5-100.

References

1. G. Wang, H. Wang, Y. Ling, Y. Tang, X. Yang, R. C. Fitzmorris, C. Wang, J. Z. Zhang and Y. Li, *Nano lett.*, 2011, **11**, 3026-3033.
2. B. Roose, S. Pathak and U. Steiner, *Chem. Soc. Rev.*, 2015, **44**, 8326-8349.
3. Y. Ding, L. Zhou, L. e. Mo, L. Jiang, L. Hu, Z. Li, S. Chen and S. Dai, *Adv. Funct. Mater.*, 2015, **25**, 5946-5953.
4. H. Xu, S. Ouyang, L. Liu, P. Reunchan, N. Umezawa and J. Ye, *J. Mater. Chem. A*, 2014, **2**, 12642-12661.
5. X. Zheng, Q. Kuang, K. Yan, Y. Qiu, J. Qiu and S. Yang, *ACS Appl. Mater. Interfaces*, 2013, **5**, 11249-11257.
6. M. D'Arienzo, J. Carbajo, A. Bahamonde, M. Crippa, S. Polizzi, R. Scotti, L. Wahba and F. Morazzoni, *J. Am. Chem. Soc*, 2011, **133**, 17652-17661.
7. D. Liao and B. Liao, *J. Photochem. Photobiol. A: Chem.*, 2007, **187**, 363-369.
8. M. Wang, J. Ioccozia, L. Sun, C. Lin and Z. Lin, *Energy Environ. Sci.*, 2014, **7**, 2182-2202.
9. X. Zhou, N. Liu and P. Schmuki, *ACS Catal.*, 2017, **7**, 3210-3235.
10. J. H. Pan, X. Z. Wang, Q. Huang, C. Shen, Z. Y. Koh, Q. Wang, A. Engel and D. W. Bahnemann, *Adv. Funct. Mater.*, 2014, **24**, 95-104.
11. S. H. Hwang, J. Yun and J. Jang, *Adv. Funct. Mater.*, 2014, **24**, 7619-7626.
12. Y. Dou, S. Zhang, T. Pan, S. Xu, A. Zhou, M. Pu, H. Yan, J. Han, M. Wei and D. G. Evans, *Adv. Funct. Mater.*, 2015, **25**, 2243-2249.
13. K. Mondal and A. Sharma, *RSC Adv.*, 2016, **6**, 83589-83612.
14. X. Lai, J. E. Halpert and D. Wang, *Energy Environ. Sci.*, 2012, **5**, 5604-5618.
15. R. Purbia and S. Paria, *Nanoscale*, 2015, **7**, 19789-19873.
16. J. Liu, S. Z. Qiao, J. S. Chen, X. W. D. Lou, X. Xing and G. Q. M. Lu, *ChemComm*, 2011, **47**, 12578-12591.
17. Z. Teng, J. Zhang, W. Li, Y. Zheng, X. Su, Y. Tang, M. Dang, Y. Tian, L. Yuwen and L. Weng, *Small*, 2016, **12**, 3473-3473.
18. C. Tian, Y. Du, H. Xu, J. Xue, W. Chu, R. Qiang, X. Han and P. Xu, *Appl. Phys. Lett.*, 2017, **111**, 133103.
19. F. Pei, L. Lin, D. Ou, Z. Zheng, S. Mo, X. Fang and N. Zheng, *Nat. Commun.*, 2017, **8**, 482.
20. A. Li, P. Zhang, X. Chang, W. Cai, T. Wang and J. Gong, *Small*, 2015, **11**, 1892-1899.
21. Z.-Q. Li, W.-C. Chen, F.-L. Guo, L.-E. Mo, L.-H. Hu and S.-Y. Dai, *Sci. Rep.*, 2015, **5**, 14178.
22. Z. Jiang, C. Zhu, W. Wan, K. Qian and J. Xie, *J. Mater. Chem. A*, 2016, **4**, 1806-1818.
23. H. Li, Z. Bian, J. Zhu, D. Zhang, G. Li, Y. Huo, H. Li and Y. Lu, *J. Am. Chem. Soc*, 2007, **129**, 8406-8407.
24. J. Feng, Y. Hong, J. Zhang, P. Wang, Z. Hu, Q. Wang, L. Han and Y. Zhu, *J. Mater. Chem. A*, 2014, **2**, 1502-1508.
25. X. Li, J. Yu and M. Jaroniec, *Chem. Soc. Rev.*, 2016, **45**, 2603-2636.
26. R. Kumar, S. Govindarajan, R. K. Siri Kiran Janardhana, T. N. Rao, S. V. Joshi and S. Anandan, *ACS Appl. Mater. Interfaces*, 2016, **8**, 27642-27653.
27. F. Zuo, K. Bozhilov, R. J. Dillon, L. Wang, P. Smith, X. Zhao, C. Bardeen and P. Feng, *Angew. Chem.*, 2012, **124**, 6327-6330.
28. C. Mao, F. Zuo, Y. Hou, X. Bu and P. Feng, *Angew. Chem. Int. Ed.*, 2014, **53**, 10485-10489.
29. S. Hoang, S. P. Berglund, N. T. Hahn, A. J. Bard and C. B. Mullins, *J. Am. Chem. Soc*, 2012, **134**, 3659-3662.
30. X. Pan, M.-Q. Yang, X. Fu, N. Zhang and Y.-J. Xu, *Nanoscale*, 2013, **5**, 3601-3614.
31. Q. Zhu, Y. Peng, L. Lin, C.-M. Fan, G.-Q. Gao, R.-X. Wang and A.-W. Xu, *J. Mater. Chem. A*, 2014, **2**, 4429-4437.
32. X. Chen, L. Liu and F. Huang, *Chem. Soc. Rev.*, 2015, **44**, 1861-1885.
33. Y. Yan, M. Han, A. Konkin, T. Koppe, D. Wang, T. Andreu, G. Chen, U. Vetter, J. R. Morante and P. Schaaf, *J. Mater. Chem. A*, 2014, **2**, 12708-12716.
34. Z. Wang, C. Yang, T. Lin, H. Yin, P. Chen, D. Wan, F. Xu, F. Huang, J. Lin and X. Xie, *Adv. Funct. Mater.*, 2013, **23**, 5444-5450.
35. X. Yu, B. Kim and Y. K. Kim, *ACS Catal.*, 2013, **3**, 2479-2486.
36. A. Sinhamahapatra, J.-P. Jeon and J.-S. Yu, *Energy Environ. Sci.*, 2015, **8**, 3539-3544.
37. H. Eskandarloo, M. Hashempour, A. Vicenzo, S. Franz, A. Badiei, M. A. Behnajady and M. Bestetti, *Appl. Catal. B Environ.*, 2016, **185**, 119-132.
38. J. Poostforooshan, A. Badiei, M. Kolahdouz and A. P. Weber, *ACS Appl. Mater. Interfaces*, 2016, **8**, 21731-21741.
39. J. Lai, S. Li, F. Wu, M. Saqib, R. Luque and G. Xu, *Energy Environ. Sci.*, 2016, **9**, 1210-1214.
40. S. De, J. Zhang, R. Luque and N. Yan, *Energy Environ. Sci.*, 2016, **9**, 3314-3347.

41. J. C. Colmenares, W. Ouyang, M. Ojeda, E. Kuna, O. Chernyayeva, D. Lisovytskiy, S. De, R. Luque and A. M. Balu, *Appl. Catal. B Environ.*, 2016, **183**, 107-112.
42. A. Ziarati, A. Badiei, G. M. Ziarani and H. Eskandarloo, *Catal. Commun.*, 2017, **95**, 77-82.
43. J. Huo, Y. Hu, H. Jiang and C. Li, *Nanoscale*, 2014, **6**, 9078-9084.
44. X. Chen, L. Liu, Y. Y. Peter and S. S. Mao, *Science*, 2011, **331**, 746-750.
45. J. Su, X.-X. Zou, Y.-C. Zou, G.-D. Li, P.-P. Wang and J.-S. Chen, *Inorg. Chem.*, 2013, **52**, 5924-5930.
46. X. Jiang, Y. Zhang, J. Jiang, Y. Rong, Y. Wang, Y. Wu and C. Pan, *J. Phys. Chem. C*, 2012, **116**, 22619-22624.
47. J. Chen, Z. Ding, C. Wang, H. Hou, Y. Zhang, C. Wang, G. Zou and X. Ji, *ACS Appl. Mater. Interfaces*, 2016, **8**, 9142-9151.
48. T. Xia and X. Chen, *J. Mater. Chem. A*, 2013, **1**, 2983-2989.
49. W. Wei, N. Yaru, L. Chunhua and X. Zhongzi, *RSC Adv.*, 2012, **2**, 8286-8288.
50. M. Sugawara, *Phys. Rev. B*, 1995, **51**, 10743.
51. M. Xing, W. Fang, M. Nasir, Y. Ma, J. Zhang and M. Anpo, *J. Catal.*, 2013, **297**, 236-243.

Supporting Information

Designer hydrogenated wrinkled Yolk@Shell TiO_2 architectures: towards advanced room temperature visible light selective photocatalysts

Abolfazl Ziarati, [a] Alireza Badiei,*[a] Rafael Luque,*[b,c] Weiyi Ouyang, [b]

[a]School of Chemistry, College of Science, University of Tehran, Tehran 1417614418, Iran

E-mail: abadiei@khayam.ut.ac.ir

[b]Departamento de Quimica Organica, Universidad de Cordoba, Campus de Rabanales, Ctra Nnal IV-A, Km 396 Edificio Marie Curie, Cordoba E-14014, Spain

E-mail: rafael.luque@uco.es

[c]Peoples Friendship University of Russia (RUDN University), 6 Miklukho-Maklaya street, Moscow, 117198, Russia

Materials and apparatus:

All the chemical reagents used in our experiments were purchased from Sigma-Aldrich and Merck and were used as received without further purification.

UV–vis DRS of samples was obtained using AvaSpec-2048 TEC spectrometer. Microscopic morphology of products was visualized by SEM (Tescan, Mira3). The compositional analysis was done by energy dispersive analysis of X-ray (EDX, Kevex, Delta Class I). Powder X-ray diffraction (XRD) was carried out on a Philips diffractometer of X'pert Company with mono chromatized Cu Kα radiation (λ = 1.5406 Å). Raman shift was recorded with a handheld Raman analyzer (Firstguard, Rigaku), that was excited by 1064 nm laser radiation. XPS measurements were performed using a VG Scientific photoelectron spectrometer ESCALAB-210 using Al Kα radiation (1486.6 eV) from an X-ray source operating at 15 kV and 20 mA.Transmission electron microscopy (TEM) was obtained on Philips CM30 with an accelerating voltage of 150 kV. High resolution transmission electron microscopy (HRTEM) was obtained on JEOL JEM 2010 - TEM under 220 KV. Textural properties of the samples were determined by N_2 physisorption using a Micromeritics TriStar II Plus. high performance liquid chromatography (HPLC, Waters Model 590 pump) equipped with a Dual Absorbance Detector (Waters 2487) and the SunFireTM C18 (3.5 _m, 150 mm length, 4.6 mm inner diameter) column provided by Waters. Gas chromatography (GC) analysis was performed using a Varian CP 3800 instrument with a flame-ionization detector (FID) using silicon DC-200 or carbowax 20 M columns.

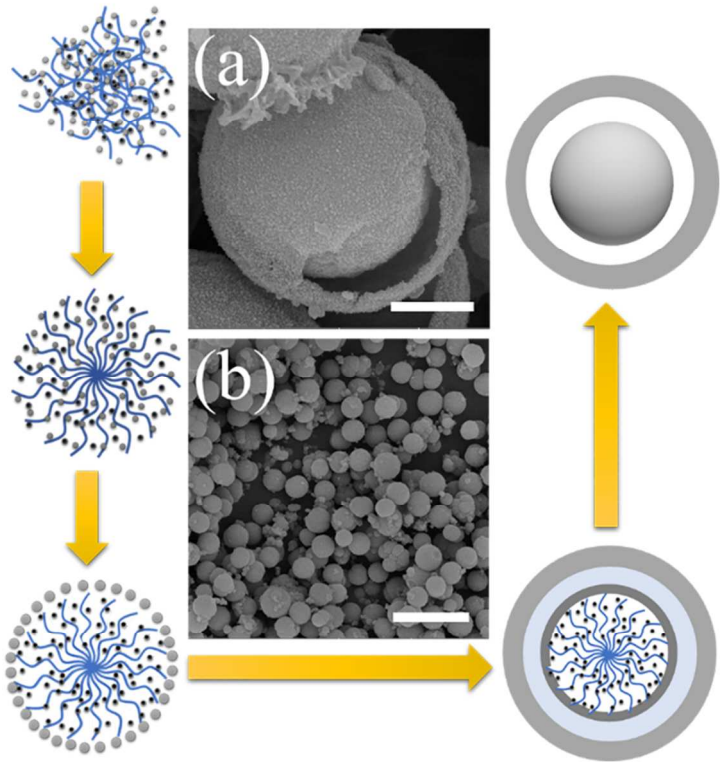

Fig. S1. Schematic diagram of the formation of Y@S-TiO_2 microspheres. The scale bar is 1μm.

The scale bars are 1 μm (a) and 10 μm (b).

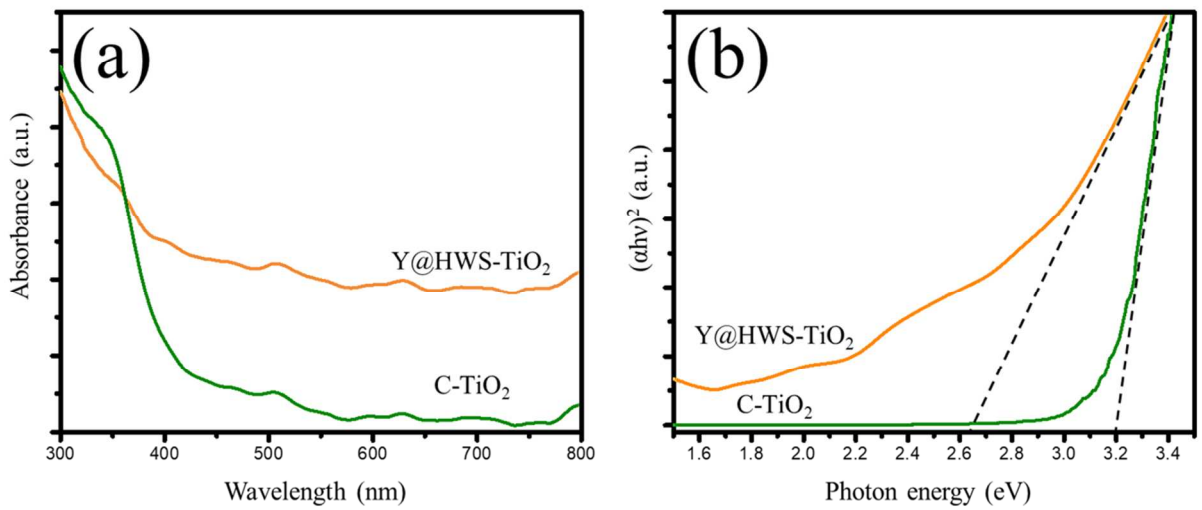

Fig. S2. UV-Vis spectra of C-TiO_2 and Y@HWS-TiO_2 (a); plot of$(\alpha h\nu)^2$ vs. *hν* for C-TiO_2 and Y@HWS-TiO_2 (b)

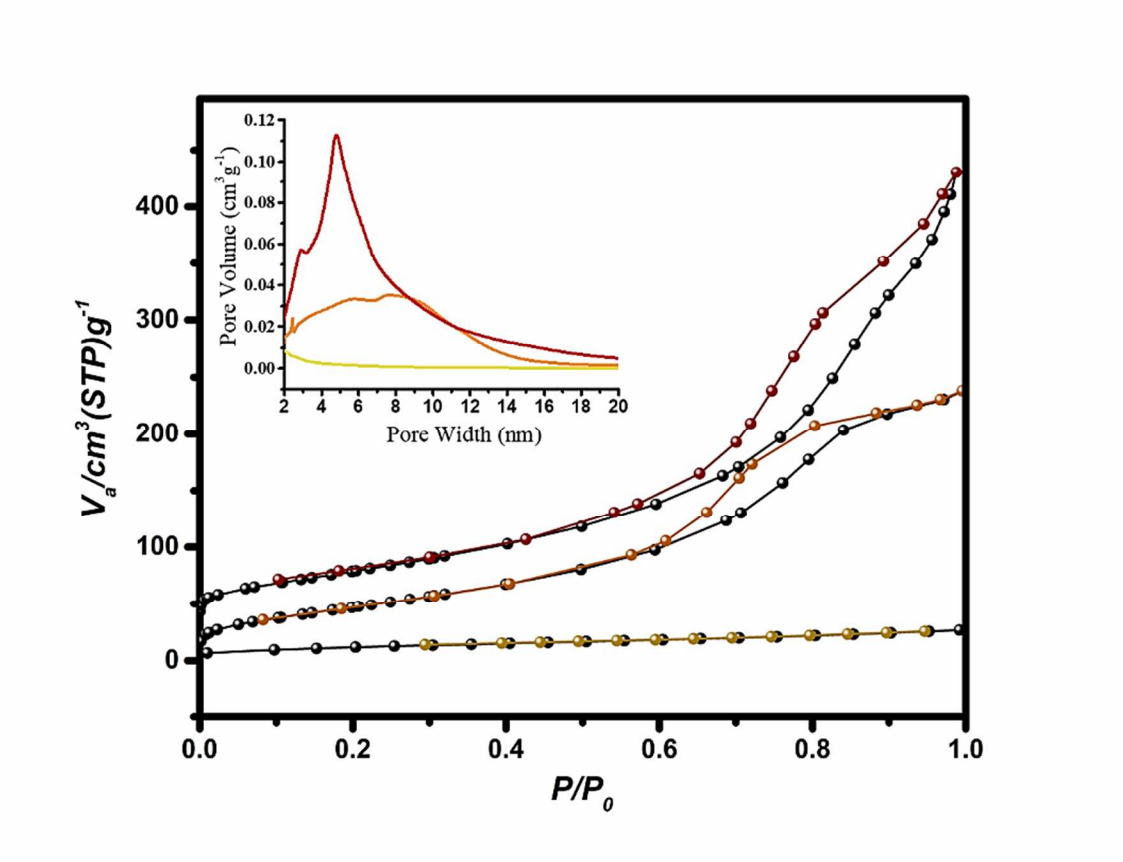

Fig. S3. Nitrogen adsorption-desorption isotherms of C-TiO_2, Y@S-TiO_2 and Y@HWS-TiO_2.

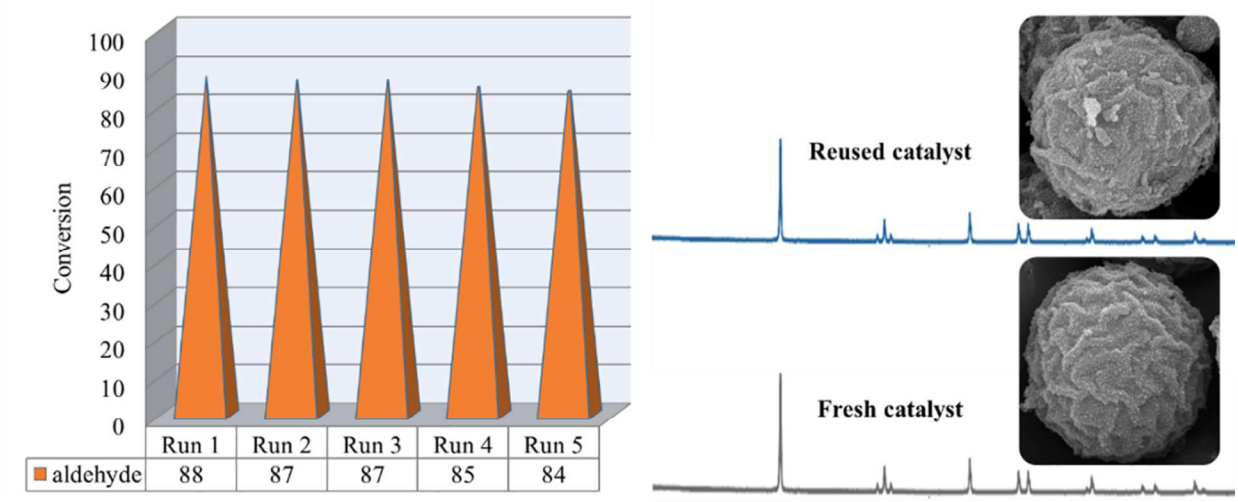

Fig. S4. Reusability study of Y@HWS-TiO_2 in the selective oxidation of benzyl alcohol.